Characterization and catalytic activity of zeolite NaY supported iridium catalysts

David M. Somerville, Michael S. Nashner, Ralph G. Nuzzo and John R. Shapley *

School of Chemical Sciences and the Frederick Seitz Materials Research Laboratory, University of Illinois at Urbana-Champaign, Urbana, IL 61801, USA

Received 9 October 1996; accepted 21 April 1997

Two catalysts were prepared (ca. 1 wt% Ir), one with metal particles located on the external surface of zeolite NaY and the other with metal particles located inside the zeolite supercages. The two catalysts exhibited very different activities and selectivities for the hydrogenolysis of *n*-butane, with the Ir *in* NaY catalyst much less active and less selective (53% ethane) than the Ir *on* NaY catalyst (83% ethane). The differences in catalytic activity and selectivity between Ir *on* NaY and Ir *in* NaY are attributed to differences in the size of the active metal particle, an ensemble effect, and not to the location (encagement) of the particle.

Keywords: iridium, NaY, butane hydrogenolysis, EXAFS

1. Introduction

The hydrogenolysis of ethane to produce two equivalents of methane is one of the simplest catalytic reactions involving a hydrocarbon and a supported metal, and it has been examined in great detail [1,2]. The hydrogenolysis of *n*-butane provides additional information concerning selectivity as well as catalytic activity. It is understood that hydrogenolysis reactions are "structure sensitive", which means that activities and selectivities can be significantly altered by slight changes in the structure of the catalytically active metal particle [3]. A full understanding of this structure sensitivity is a desirable goal. Zeolite supported metal catalysts are particularly interesting, since the traditional functions of an oxide support, viz., limiting metal particle aggregation or providing a proton source in bifunctional systems [4], are supplemented by the size and shape selectivity enforced by the well-defined zeolite lattice [5–11].

The formation of iridium carbonyl clusters ($Ir_4(CO)_{12}$ or $Ir_6(CO)_{16}$) inside the supercages of zeolite NaY by controlled reduction (CO/H_2) of an ion-exchanged zeolite has been extensively reported [12–16]. It has recently been shown that it is possible to form these same materials from the reduction of an organometallic precursor that has been absorbed by the zeolite [17]. The use of organometallic precursors allows the formation of metal clusters and, through subsequent activation, metal particles inside the supercages of NaY without acidification of the zeolite.

We believed it would be of general interest to examine the properties of two distinctly different catalysts involving zeolite NaY and Ir: one derived from $Ir_4(CO)_{12}$ selectively placed on the external surface of the zeolite matrix and the other derived from $Ir_4(CO)_{12}$ formed inside of the zeolite framework. Activation of these materials in H_2 at 773 K was expected to lead to two compositionally similar catalysts which could be compared on the basis of particle size and location. We have found in the hydrogenolysis of *n*-butane by these catalysts, the one derived from $Ir_4(CO)_{12}$ *on* NaY is much more active and selective than the one derived from $Ir_4(CO)_{12}$ *in* NaY. Extensive characterization of these two systems through infrared spectroscopy of chemisorbed CO, scanning transmission electron microscopy, and X-ray absorption spectroscopy indicates that the observed catalytic differences are caused by ensemble effects and are not due to electronic effects or shape selective properties imposed by the zeolite support.

2. Experimental

2.1. Catalyst preparation

The preparation of $Ir_4(CO)_{12}$ *in* NaY (ca. 1 wt% Ir) was performed using a modified literature procedure [17] with standard Schlenk line techniques. Typically, 20 mg of $Ir(CO)_2$acac (acac = acetylacetonate), prepared by literature methods [18] and purified by sublimation, was dissolved in 20 ml of dry hexane and introduced under N_2 to 1 g of zeolite NaY (LZ-Y52, Union Carbide), which had been treated under vacuum at 100°C for ca. 2 h. Adsorption of $Ir(CO)_2$acac by the zeolite was complete within 5 to 10 min as indicated by the disappearance of the yellow color of the solution. The infrared spectrum of the supernatant then displayed no CO bands. After stirring the slurry for 30 min, the

* To whom correspondence should be addressed.

supernatant was removed by cannula and the zeolite was dried under vacuum for 2 h (25°C). The iridium containing zeolite was exposed to flowing CO for 10 to 12 h at 25–40°C until the sharp, characteristic CO bands of $Ir_4(CO)_{12}$ *in* NaY (2068, 1925 cm^{-1}) were observed in the infrared spectrum of the material (KBr pellet, ca. 5 mg zeolite/300 mg KBr). Attempts to extract $Ir_4(CO)_{12}$ from the zeolite with refluxing chlorobenzene or with a solution of $N(PPh_3)_2^+Cl^-/CH_2Cl_2$ were unsuccessful, confirming encapsulation of the iridium cluster.

The preparation of $Ir_4(CO)_{12}$ *on* NaY (ca. 1 wt% Ir) was performed by the addition of 1 g of dried zeolite (vide supra) to a slurry of ca. 17 mg of $Ir_4(CO)_{12}$ dispersed in 50 ml of cyclohexane. The slurry was stirred for 1 h before the solvent was removed under vacuum and the zeolite dried under vacuum for another 2 h (25°C). Weight percent loadings of Ir were established by elemental analysis.

2.2. Catalytic studies

The zeolite supported iridium samples (ca. 250 mg) were activated and tested on a catalyst line that includes a gas handling system, catalytic reactor, and equipment for analysis of the effluent [19,20]. Streams of hydrogen (Matheson, 99.999%) and *n*-butane (Matheson, 99.0%) were deoxygenated over Cr(II)/SiO_2 and dried over activated molecular sieves. The Pyrex U-tube reactor contained a course frit supporting the catalyst bed, which was in contact with a thermocouple well containing an Omega type-k chromel/alumel thermocouple. The reactor was heated by a tube furnace controlled with an Omega CN2011 temperature controller. A Packard model 430 gas chromatograph with a flame ionization detector was used to separate and quantify the hydrocarbon products ($1/8'' \times 7'$, 10 wt% *n*-octane/Porasil column).

Prior to activation, each sample was flushed with H_2 for 15 to 30 min to displace any air introduced into the system while loading the catalyst. The samples were activated by heating to 773 K (at 15 K/min) under a stream of H_2 (40 ml/min) and holding at 773 K for 1 h. The samples were cooled to the appropriate temperature under a continuous stream of H_2 and *n*-butane was introduced into the gas flow ($H_2/C_4H_{10} = 40/4$ ml/min). Arrhenius plots were constructed from data collected at temperatures for which the conversion of *n*-butane was held below 10% (450–575 K). Before collecting data at a new temperature the catalyst was cleaned by heating in H_2 to 773 K and holding for 1 h. The catalyst was then cooled to the desired temperature and the process repeated.

2.3. Infrared spectroscopy

Supported samples for infrared studies were prepared as described above and were pressed into wafers (75–100 mg, 2 cm diameter, 3700 psi) suitable for infrared transmittance studies. The wafers were loaded into a temperature-controlled infrared cell (Harrick Scientific model HTC-100), having KBr windows sealed with Viton o-rings, which was then purged with H_2. Samples were heated to 723 K in H_2 and held for 1 h. The samples were then cooled to ambient temperatures and placed under vacuum for ca. 1 h before being flushed with He and sealed in a CO atmosphere for ca. 4 h. The sample was evacuated and infrared spectra recorded with a Perkin-Elmer 1750 FT-IR spectrometer. Background spectra were determined from a zeolite wafer treated in an analogous fashion.

2.4. X-ray absorption spectroscopy (XAS)

All XAS measurements were performed in a Lytle-style catalyst cell (the EXAFS Company). The cell allowed in situ X-ray fluorescence measurements with an operating temperature up to 773 K. A metered flow of H_2 (Matheson, 99.999%) was passed through traps to remove oxygen and water before entering the cell. To avoid oxygen contamination during the experiments, the volume surrounding the sample was continuously purged with H_2, and the shielding volume surrounding the reactor was purged with He (Matheson, 99.995%). Previously prepared, unactivated, catalyst samples (ca. 150 mg) were pressed into a pellet (1 mm × 10 mm). The pellet was fastened to the sample mount of the Lytle cell, and the cell was purged with H_2 for 1 h. The temperature was monitored with an Omega type-k chromel/alumel thermocouple mounted directly on the sample stage. The supported samples were activated by heating them at 15 K/min in flowing H_2 (40 ml/min) to a temperature of 773 K and holding at that temperature for 1 h. The samples were cooled to room temperature before making the EXAFS measurements.

Fluorescence EXAFS data were taken on the Ir L_3-edge of the catalyst samples. Transmission EXAFS data were taken at room temperature on the Pt L_3-edge of the reference compounds PtO_2 and Pt metal dispersed on Kapton tape. The thickness of the reference compounds was approximately 4 μm as determined optically with a microscope.

X-ray absorption data were measured at the National Synchrotron Light Source, located at Brookhaven National Laboratory, Upton, New York, on the UIUC/AT&T beamline X16C. The X16C beamline uses a sagitally-focusing Si(111) crystal monochromator, which focuses 3.5 mrad of light into a 0.3 mm × 1 mm beam spot at the sample. The focusing dynamically follows the energy to maintain the beam spot profile over the scan. The initial beam intensity I_0 was measured with a six-inch ion chamber containing a 1 : 1 mixture of He and N_2. The fluorescence was measured with a Lytle detector filled with Ar and placed at 90° to the incident beam. Before taking data on each sample, the energy of the beam was calibrated to the

Table 1
Hydrogenolysis of *n*-butane [a]

Catalyst	E_a (kJ/mol)	Temp. range (K)	Rate [b] at 473 K	% Methane at 473 K	% Ethane at 473 K	% Propane at 473 K
Ir *on* NaY (0.8 wt%)	177 (10)	436–474	0.8 (2)	8.9	83.2	7.8
	197 (5)	438–475	0.69 (8)	8.9	83.2	7.8
Ir *in* NaY (0.8 wt%)	186 (15)	468–519	0.021 (9)	25.7	52.5	21.6
Ir *in* NaY (1.7 wt%)	185 (2)	455–508	0.025 (1)	25.2	50.0	24.7

[a] Values in parentheses are uncertainties at one standard deviation.
[b] Rate = mol C_4/mol Ir per min.

inflection point of the Re L_3-edge threshold by using a sample of Re metal.

The EXAFS data analysis was performed by following the technique of Kinkaid et al. [22,23]. The background was subtracted in *k*-space by using a least-squares fit to a cubic spline function with two knots. The Fourier-filtered, k^2-weighted data were fit by non-linear least-squares to a three-shell model to determine the average coordination number, *N*, the nearest neighbor distances, *R*, the change in the threshold energy, ΔE_0, and the Debye–Waller factor, $\Delta\sigma^2$, for each shell in *k*-space. A Hanning window function was used to select the shells for analysis. Ir–Ir scattering was modeled using the Pt–Pt scattering function taken from Pt metal. A Pt–O absorber–scatterer pair from PtO_2 was used to model the Ir–O scattering function.

For the Ir L_3 XANES data, the step height was normalized by straight line fits to the pre-edge and post-edge (> 100 eV) regions.

2.5. Scanning transmission electron microscopy (STEM)

Images were obtained on a Vacuum Generators HB501 STEM operating at 100 keV. Samples were prepared by dipping a carbon grid into a vial of previously activated catalyst and shaking off the visibly excess material.

3. Results

3.1. Hydrogenolysis of n-butane

The catalytic activities of Ir *on* NaY and Ir *in* NaY are summarized in table 1. Arrhenius plots were constructed from the reaction rate (mol *n*-butane/mol Ir per min) measured at several temperatures (figure 1). Ir *in* NaY and Ir *on* NaY were found to have similar activation energies with calculated values near 190 kJ/mol. Comparison of the normalized reaction rates at 473 K shows Ir *on* NaY is approximately 30–40 times more active than Ir *in* NaY for the hydrogenolysis of *n*-butane. Product selectivities for the two catalysts are shown in figure 2. The Ir *on* NaY catalyst is highly selective towards ethane, whereas Ir *in* NaY is only slightly selective towards ethane. Product selectivity is relatively independent of reaction temperature for Ir *on* NaY while product distribution becomes more random with increased reaction temperature for Ir *in* NaY.

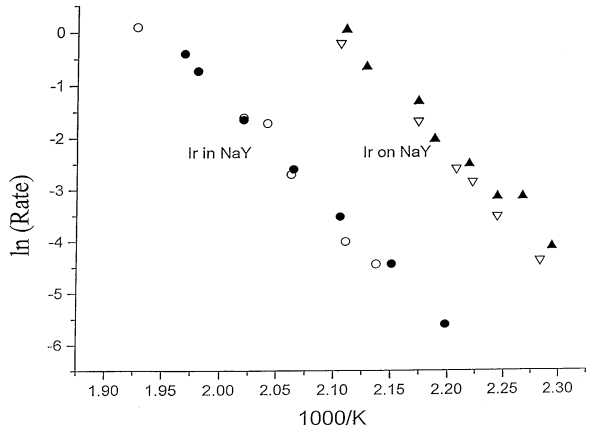

Figure 1. Arrhenius plots for the hydrogenolysis of *n*-butane. Ir *on* NaY (open and closed triangles, separate catalyst samples, both 0.8 wt%); Ir *in* NaY (open circles = 0.8 wt%, closed circles 1.7 wt%). Rate = (mol butane reacted)/(mol Ir) per min.

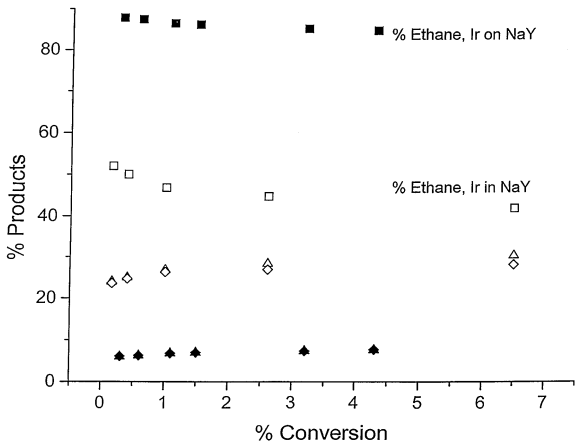

Figure 2. Selectivity profiles for the hydrogenolysis of *n*-butane by Ir *on* NaY (open symbols) and Ir *in* NaY (closed symbols): methane (triangles), ethane (squares), propane (diamonds).

Comparison of the amounts of methane relative to propane indicate hydrogenolysis of a single carbon–carbon bond is occurring in most cases (vide infra). Ir *in* NaY was found to be relatively insensitive to wt% loadings of Ir with respect to activity (on a per Ir basis) and selectivity.

3.2. Infrared spectroscopy of chemisorbed CO

The infrared spectra of CO chemisorbed on activated Ir *on* NaY and Ir *in* NaY is given in figure 3. The spectrum for Ir *on* NaY shows a strong CO band at 2067 cm^{-1} with a shoulder near 2025 cm^{-1} while that of Ir *in* NaY is much more complex (2130 (w), 2099 (sh), 2085 (vs), 2066 (s), 2060 (s), 2040 (s), 1816 (m)). The spectrum of Ir *in* NaY is labelled at 2099, 2085, and 2040 cm^{-1}.

3.3. X-ray absorption spectroscopy, EXAFS and XANES

Figure 4 compares the Fourier-transformed EXAFS data (not phase corrected) for Ir *on* NaY and Ir *in* NaY (k-range ca. 3.5–13.0 $Å^{-1}$) from which the filtered data (indicated by brackets) were taken and used for the fitting procedure. The most striking feature in the radial structure functions is the difference in the magnitude of the first metal-shell between the two samples. The first metal-shell for Ir *on* NaY is approximately three times larger than the first metal-shell of Ir *in* NaY. Ir *on* NaY also has a significant amount of higher shell structure which is absent in Ir *in* NaY. Qualitatively, this indicates the Ir particles of Ir *on* NaY are much larger and show a greater degree of order than the Ir particles of Ir *in* NaY (vide infra).

Quantitative structural parameters from the first-shell EXAFS data of the catalyst material were extracted by fitting the Fourier-filtered Ir EXAFS data, with the phase shift and amplitude functions determined from bulk Pt metal and PtO_2 as model compounds. The bracket in figure 4 indicates the limits of the Hanning window function used to isolate and Fourier-filter the first-shell data. Because of the overlap of the first metal-shell and the low-Z shells, they were analyzed together using a three-shell model. The Fourier-filtered data, along with the appropriate fits and residuals, are shown in figure 5.

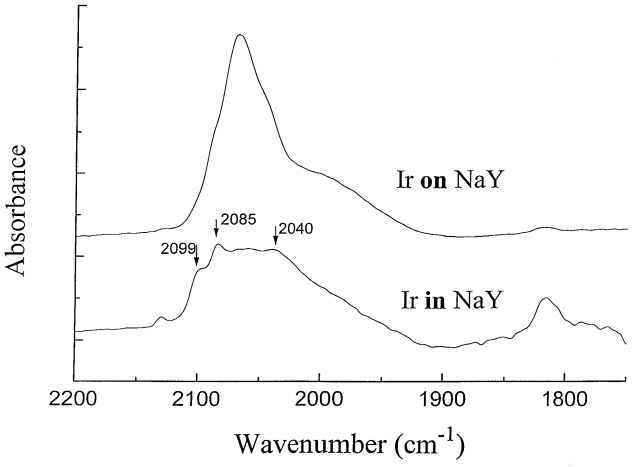

Figure 3. Infrared spectra of CO chemisorbed onto Ir *on* NaY and Ir *in* NaY. The spectrum of Ir *in* NaY is labelled with arrows at 2099, 2085, and 2040 cm^{-1}.

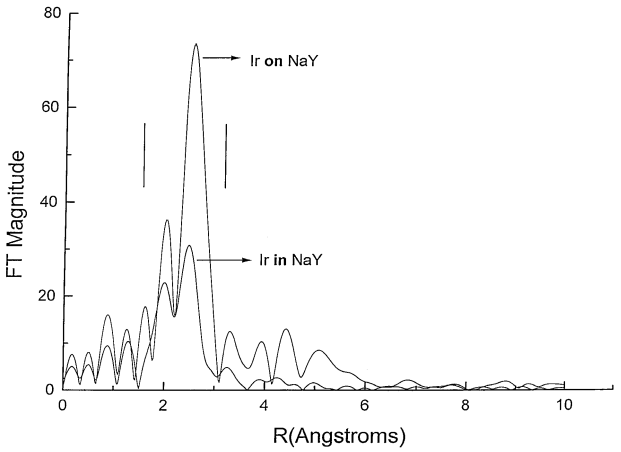

Figure 4. Comparison of the Fourier-transformed, k^2-weighted EXAFS data for the Ir L_3-edge of activated Ir *on* NaY and Ir *in* NaY collected at 300 K (k = ca.3.0–13.0 $Å^{-1}$). The bracket shown in each figure indicates the limits of the Hanning filter used to select the first shells in the analysis.

The best fit to the Ir *on* NaY EXAFS data was obtained using a three-shell fit with 8.7 Ir–Ir scatterers at 2.70 Å and minimal contributions from two Ir–O scatterers. The best fit to the Ir *in* NaY EXAFS data was obtained using a three-shell fit with 3.2 Ir–Ir scatterers at 2.68 Å, 3.5 Ir–O scatterers at 2.55 Å and 0.2 Ir–O scatterers at 2.13 Å. Fitting results for both catalysts are presented in table 2.

The higher shell structure observed for Ir *on* NaY in figure 4 indicates that three-dimensional particles of fcc packed Ir are formed during activation. Specifically, shells are seen at 2.51 (R_1), 4.41 (R_3), and 5.07 Å (R_4), which correspond to bulk Ir metal with 12 nearest neighbors at 2.715 Å (R_1), 24 neighbors at 4.702 Å (R_3), and 12 neighbors at 5.430 Å (R_4). A shell at R_2 (6 neighbors at 3.84 Å in bulk Ir) in the radial structure function is not readily assigned as it is obscured by the multiple scattering interactions observed at 3.29 and 3.93 Å. By truncating the data over a slightly different k range (4–12 $Å^{-1}$), the assignment of a shell at R_2 is readily made (figure 6). It is generally agreed that the presence of a shell at R_2 is a key indicator of a three-dimensional particle as opposed to a two-dimensional particle [23,24].

The magnitude of the first metal shell can be correlated with metal particle size [25–29]. Assuming a three-dimensional particle morphology for the Ir particles of

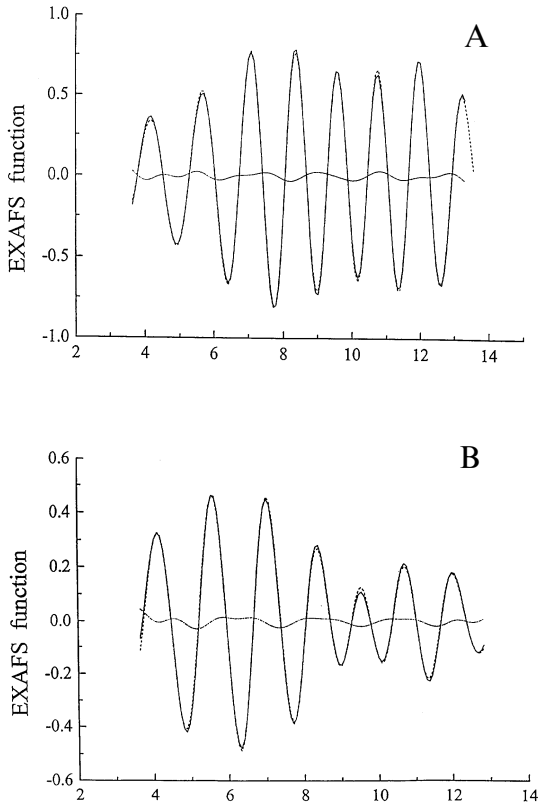

Figure 5. Fourier-filtered data (1.8–3.2 Å), solid line, with corresponding fits, broken line, and residuals, dashes, for (A) Ir *on* NaY and (B) Ir *in* NaY.

Ir *on* NaY, an average particle size of 2.0–2.5 nm is estimated from the first-metal-shell coordination number. Similar Ir particles ($N = 8.5$) supported on silica have been estimated to contain 100 atoms [30]. The first-metal-shell coordination number of 3.2 found for Ir *in* NaY suggests the Ir particles formed after activation contain 4 to 6 Ir atoms and have an average particle size of ca. 0.8 nm [17,30b,31,32].

The XANES data (figure 7) suggests the Ir particles of activated Ir *in* NaY and Ir *on* NaY are electronically similar, since the intensities and position of the white lines are the same within 5%.

Table 2
EXAFS fitting results for Ir *on* NaY and Ir *in* NaY

		N [a]	R [b] (Å)	ΔE_0 [c]	$\Delta\sigma^2$ [d]
Ir *on* NaY	Ir–Ir	8.74	2.70	1.25	−0.0019
	Ir–O	0.78	2.53	−3.29	−0.0027
	Ir–O	0.07	2.08	−7.00	−0.0089
Ir *in* NaY	Ir–Ir	3.23	2.68	8.30	−0.0032
	Ir–O	3.57	2.55	−1.78	−0.0099
	Ir–O	0.20	2.13	−9.68	−0.0077

[a] Average coordination number.
[b] Nearest neighbor distance.
[c] Relative absorption energy.
[d] Relative Debye–Waller factor.

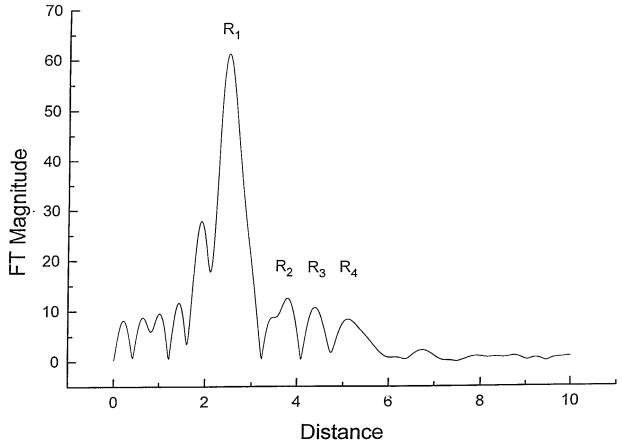

Figure 6. Fourier-transformed, k^2-weighted EXAFS data for the Ir L_3-edge of Ir *on* NaY (k range 4–12 Å^{-1}).

3.4. Scanning transmission electron microscopy (STEM)

STEM images for activated Ir *on* NaY and Ir *in* NaY are given in figure 8. The STEM image of Ir *on* NaY shows the presence of highly dispersed Ir particles which are roughly 2 nm in diameter. The STEM of Ir *in* NaY is relatively barren, indicating the occlusion of small Ir particles inside the zeolite. No regions containing large Ir particles (> 3 nm) were observed for Ir *in* NaY.

4. Discussion

4.1. Catalyst characterization

4.1.1. Particle structure

The infrared spectra of CO chemisorbed on the activated catalysts shows the Ir particles of Ir *on* NaY (2067 cm^{-1}) and Ir *in* NaY (2085, 2066, 2060,and 2040

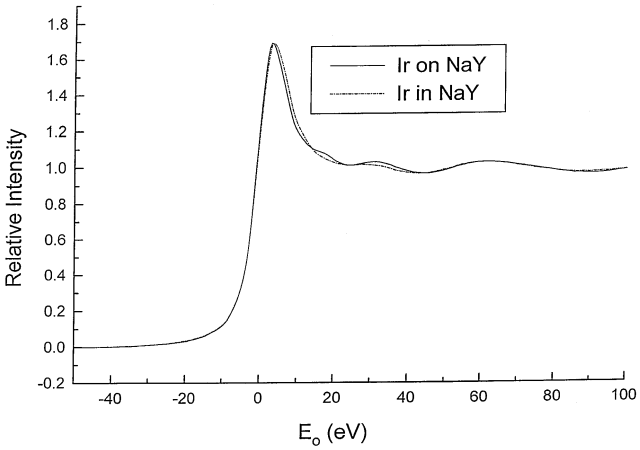

Figure 7. Comparison of the XANES data for the Ir L_3-edge of Ir *on* NaY (dashed line) and Ir *in* NaY (straight line).

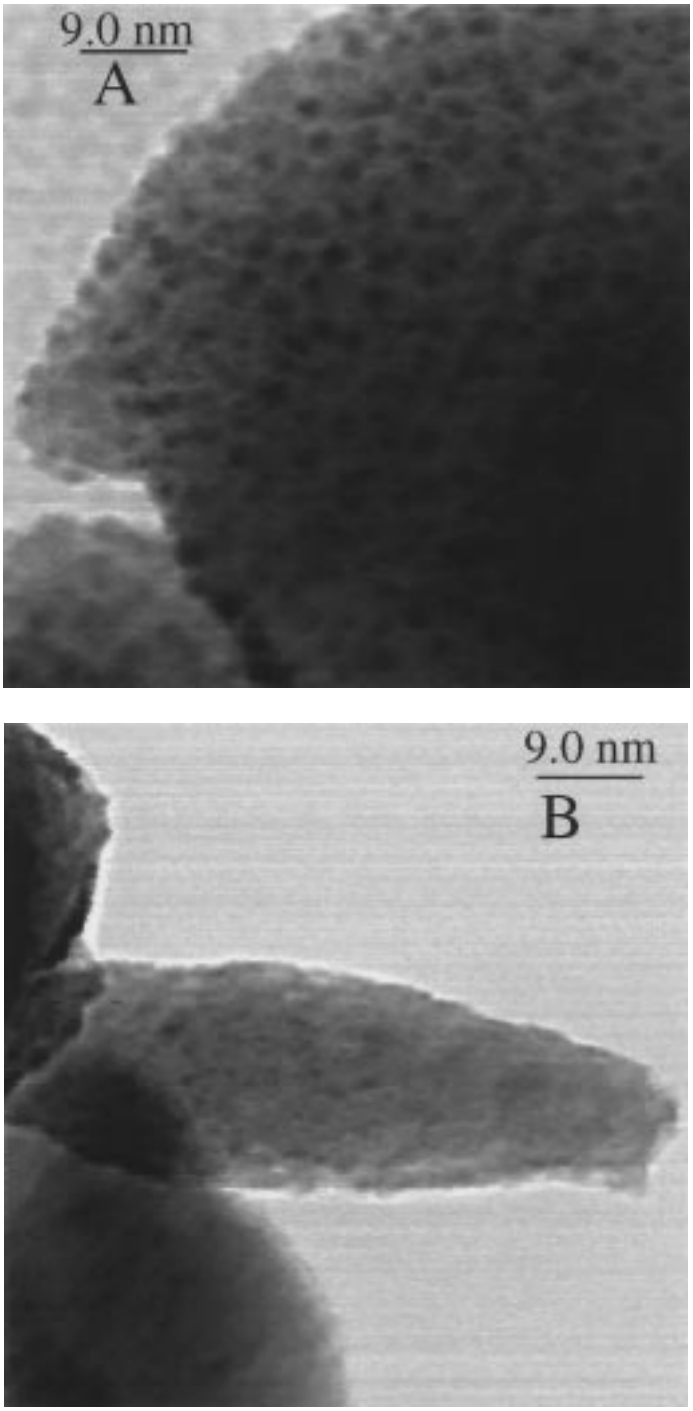

Figure 8. STEM images ($X = 2 \times 10^6$) of activated (A) Ir *on* NaY and (B) Ir *in* NaY.

cm^{-1}) to be highly dispersed, as indicated by the dominance of high-frequency terminal carbonyl groups [33]. The more complicated spectra exhibited by Ir *in* NaY could well reflect a distribution of Ir environments within the zeolite or possibly interactions between the carbonyls and the zeolite walls [34,35].

The EXAFS data of Ir *on* NaY is very similar to EXAFS studies of highly dispersed Ir supported on either alumina or silica [36,37]. Both types of Ir particles show a large first-metal-shell feature as well as higher metal-shell structure. Depending upon the method of preparation, first-metal-shell coordination numbers of 6 to 11 are commonly reported for Ir particles formed on amorphous supports. The Ir–Ir bond distance of 2.70 Å and the low Debye–Waller factor found for the Ir particles of Ir *on* NaY agree with reported literature values for Ir supported on silica and alumina as well. A three-dimensional, fcc close packed model is proposed for the

Ir particles of Ir *on* NaY based upon the higher shell structure seen in the Fourier-transformed EXAFS data. This conclusion is consistent with reports of Ir on amorphous supports where it was concluded that the particles are more nearly spherical than "raft-like" [24].

Similarly, the EXAFS data of Ir *in* NaY resembles the EXAFS data reported for other Ir particles dispersed within zeolites [17,30b,31,32]. A comparison of fitting results is provided for the Ir particles of Ir *in* NaY with the highly dispersed, zeolite supported Ir particles described by Gates (table 3). The Ir particles of Ir *in* NaY are quite similar to those reported by Gates, which were formed via the decarbonylation of $Ir_4(CO)_{12}$, $Ir_6(CO)_{16}$ and $Ir_4(CO)_{11}^-$ encaged within zeolites NaY and NaX in H_2 at 573 K. The Ir particles formed from the reduction of an ion exchanged KLTL zeolite were found to be of comparable size as well to that of the particles reported in this study. The systems summarized in table 3 all show a low first-metal-shell coordination and a significant interaction of Ir centers with the support. These particles are best described as 4 to 6 Ir atom clusters.

The particle sizes estimated from EXAFS suggests the Ir particles of Ir *on* NaY should be located on the external surface of the zeolite while the Ir particles of Ir *in* NaY are small enough to reside in the zeolite supercage. These conclusions have been confirmed by STEM images, which show highly dispersed, ca. 2 nm particles supported on the external surface of the zeolite are present for Ir *on* NaY, whereas very few observable features are present for Ir *in* NaY.

4.1.2. Particle electronic state

The similarity of the absorption threshold resonance in the XANES data for the Ir L_3-edge obtained for these systems indicates the Ir particles of Ir *in* NaY and Ir *on* NaY have very similar electronic states. X-ray absorption edge studies have proven useful in the examination of the electronic structure of supported metal catalysts, as the absorption threshold resonance can be directly related to the electron population of the outer d orbitals of the metal [38]. Variation in the electronic structure of the metal with changes in particle size is expected, as highly dispersed metals have a greater amount of support interactions. However, the difference is often slight and frequently not above the limits of uncertainty of the XANES measurements [38]. A change in the absorption threshold resonance with metal particle size has been observed for Ir particles supported on MgO [39], but not for Ir particles supported on alumina and silica. Thus, XANES does not rigorously exclude the possibility of electronic differences between Ir *on* NaY and Ir *in* NaY, but the results do indicate that such differences, if present, are rather subtle.

Table 3
Comparison of Ir *in* NaY EXAFS fitting results with other highly dispersed (ca. 1 wt%) Ir/zeolite catalysts

Catalyst	*N* Ir–Ir	*N* Ir–O (total)	Treatment	Ref.
Ir *in* NaY	3.2	3.77	773 K, H_2	this work
$[Ir_6]$/NaY	3.6	2.86	573 K, H_2	[17]
$[Ir_4]$/NaX	3.0	3.05	573 K, H_2	[32]
Ir/KLTL	3.2	3.7	573 K, H_2	[31]
	4.2	1.9	773 K, H_2	

The infrared spectrum of chemisorbed CO is often used as a probe of the electronic state of a supported metal particle [35]. The stretching frequency of the CO band is used as an indirect measure of the metal particle electron density, as this is believed to be directly related to the ability to donate electrons to the CO π^* level. It should also be realized that the location and intensities of the CO bands will also be highly sensitive to the morphology of the metal particle in addition to its electronic state. The infrared spectra for chemisorbed CO reported in this study do not appear to give significant insights regarding the electronic nature of the supported iridium particles. The Ir particles of Ir *in* NaY cannot be assigned as either electron rich or electron deficient with respect to the Ir particles of Ir *on* NaY, as the former exhibits CO bands that are both higher in wavenumber and lower in wavenumber than the CO band at 2067 cm^{-1} seen for the latter.

We have been unable to show that any major electronic differences exist between the metal particles in these two systems. In contrast, we have been able to show that dramatic differences exist concerning the size and morphology of the Ir particles found in Ir *on* NaY in comparison to Ir *in* NaY. We therefore believe the catalytic differences exhibited by these two systems are the result of structural effects rather than electronic effects.

4.2. Hydrogenolysis of n-butane

An important aspect of the hydrogenolysis data is the mass balance of the various products arising from C–C bond cleavage. For hydrogenolysis reactions using Ir *in* NaY, mass transfer limitations could significantly complicate the interpretation of the data, especially the selectivity of the catalyst, since secondary reactions of the hydrocarbon are more likely to occur when intraparticle diffusion rates in the zeolite lattice approach the reaction rate. For the butane system, however, the conditions used in this study yield equal molar amounts of methane and propane (figure 2). Thus, the secondary conversion of ethane to methane or of propane to methane and ethane can be discounted, and the kinetic parameters measured can be assumed to be intrinsic ones.

The activation energies calculated for Ir *on* NaY and Ir *in* NaY are similar to other reports of the hydrogenolysis of *n*-butane by supported Ir [40–47]. The high activity and selectivity to ethane exhibited by Ir *on* NaY is typical for highly dispersed Ir particles [40] and is consistent with the structural description provided for the Ir particles in this system. The low selectivity towards

ethane exhibited by Ir *in* NaY is typical of large (3–4 nm) Ir particles [40], a situation which is not consistent with the structural description deduced for the Ir particles of Ir *in* NaY. In addition, while the selectivity of *n*-butane hydrogenolysis is known to be sensitive to the Ir particle size, the reaction rate, expressed on a per surface iridium basis, was found to be independent of this parameter over a particle size range of 1 to 7 nm (determined by electron microscopy) [40]. Again, this is inconsistent with the observed activities as Ir *on* NaY was found to be much more active than Ir *in* NaY.

Despite a significant amount of study concerning the hydrogenolysis of *n*-butane by Ir [40–49], the mechanism which leads to the high selectivity towards ethane displayed by small Ir particles is not understood. Comparison of the activation energies for a series of alkanes led to the suggestion that Ir particles adsorb *n*-butane in a "C_2 unit" mode by adsorption at two adjacent carbon atoms and that as particle size changed so did the preferred mode of C_2 unit adsorption [40]. Single crystal studies have led to the suggestion that small Ir particles display a large selectivity to ethane as the result of a mechanism involving a sterically demanding metallocyclopentane intermediate that forms at single Ir centers [43].

Our initial goal in this study was to exploit the shape selectivity of the zeolite support to perhaps disfavor the formation of a metallocyclopentane or a certain C_2 unit mode of adsorption. However, the dramatic loss of catalytic activity for the Ir *in* NaY system suggests we are actually observing the results of an ensemble effect. Previous studies have indicated that a minimum number of adjacent, catalytically active metal atoms are required to efficiently catalyze the hydrogenolysis of hydrocarbons [50,51]. This minimum ensemble of atoms is the number of atoms required to abstract H atoms from the hydrocarbon, provide an adsorption site for the olefinic intermediate, break the C–C bond, and hydrogenate the resulting surface species to form lower molecular weight hydrocarbons. It has been reported that the chemisorption of ethane involves ca. five contiguous metal atoms [51,52], while the complete hydrogenolysis of ethane requires a larger ensemble of ca. 12 metal atoms [51–54]. Similarly, the complete hydrogenolysis of *n*-butane is reported to require ca. 20–24 metal atoms [54], but the partial hydrogenolysis (breaking a single C–C bond) should not require an ensemble substantially larger than that required for the hydrogenolysis of ethane. Although the absolute number of atoms required in such an ensemble, and whether or not the ensemble size is element specific, is open to debate, it is noted that the suggested ensemble of 12 metal atoms is twice as large as the 4–6 metal atom particles of Ir *in* NaY and is much smaller than the 100 metal atom particles of Ir *on* NaY. This estimate of critical ensemble size lends support to the idea that the hydrogenolysis of *n*-butane by Ir *in* NaY is ensemble size limited.

There is a large body of literature that suggests electronic effects, both inherent in the metal particle and induced by the support [55], play a dominant role in reactions catalyzed by supported metals. Gates has observed that very small Ir particles supported on MgO have lower activity in propane hydrogenolysis compared to larger Ir particles [56]. Gates has also observed that small Ir particles supported on various oxides have lower activity in structure insensitive reactions (hydrogenation) compared to larger Ir particles [57]. It was noted that the small Ir particles interacted with H_2 more strongly than did larger Ir particles and that this was probably due to electronic differences between the two [57]. While electronic differences between Ir *on* NaY and Ir *in* NaY may be responsible for some of the catalytic differences observed in these systems, our failure to detect such differences leads us to conclude that structural factors are more important than electronic ones.

5. Conclusions

Two heterogeneous catalysts have been prepared, one derived from $Ir_4(CO)_{12}$ supported on zeolite NaY and one derived from $Ir_4(CO)_{12}$ supported in NaY. The two catalysts behaved quite differently in a structure sensitive reaction, the hydrogenolysis of *n*-butane, with Ir *on* NaY displaying a greater activity and selectivity than Ir *in* NaY. Extensive characterization of these two systems by IR, STEM, and EXAFS has revealed two structurally different systems with the Ir particles of Ir *on* NaY much larger and with a greater degree of order than the Ir particles of Ir *in* NaY. XANES has demonstrated negligible differences exist between the electronic states of the Ir particles in these systems. In contrast to the large body of literature which has focused on the electronic properties of zeolite supported metal catalysts, we are compelled to argue the catalytic differences exhibited by these two systems are based upon ensemble effects and not electronic or encagement effects.

Acknowledgement

This research was supported by grants from the US Department of Energy, grant No. DEFG02-96ER45339, and the National Science Foundation, grant No. DMR 89-20538. STEM images were obtained at the Center for Microanalysis of Materials, University of Illinois, which is supported by the US Department of Energy under grant DEFG02-91-ER45439. The authors appreciate the in situ Lytle cell made available by Exxon and the donation of NaY by Dr. W. Wachter from Exxon Research and Development Laboratory.

References

[1] J.A. Dumesic, D.F. Rudd, L.M. Aparicio, J.E. Rekoske and A.A. Treviño, *The Microkinetics of Heterogeneous Catalysis* (ACS, Washington, 1993) ch. 7.
[2] J.H. Sinfelt, Catal. Rev. Sci. Eng. 3 (1969) 175.
[3] M. Che and C.O. Bennet, *Advances in Catalalysis*, Vol. 36 (Academic Press, London, 1989) p. 55.
[4] C.N. Satterfield, *Heterogeneous Catalysis in Industrial Practice* (McGraw-Hill, New York, 1991).
[5] S.M. Csicsery, Zeolites 4 (1984) 202.
[6] N.Y. Chen, T.F. Gegnan and C.M. Smith, eds., *Molecular Transport and Reaction in Zeolites – Design and Application of Shape Selective Catalysts* (VCH, New York, 1994).
[7] M. Ichikawa, *Advances in Catalysis*, Vol. 38 (Academic Press, London, 1992) p. 283.
[8] W.M.H. Sachtler and Z. Zhang, *Advances in Catalysis*, Vol. 39 (Academic Press, London, 1993) p. 129.
[9] C.P. Nicolaides and M.S. Scurrell, in: *Keynotes in Energy-Related Catalysis*, ed. S. Kaliaguine (Elsevier, Amsterdam, 1988) ch. 6.
[10] S. Kawi and B.C. Gates, in: *Clusters and Colloids*, ed. G. Schimd (VCH, New York, 1994) ch. 4.
[11] L. Sordelli, G. Martra, R. Psaro, C. Dossi and S. Coluccia, J. Chem. Soc. Dalton Trans. (1996) 765.
[12] F. Lefebvre, P. Gelin, B. Elleuch, Y. Diab and Y. Ben Taârit, in: *Structure and Reactivity of Modified Zeolites*, eds. P.A. Jacobs, N.I. Jaeger, P. Jírú, V.B. Kazansky and G. Schulz-Ekloff (Elsevier, Amsterdam, 1984) pp. 257–272.
[13] G. Bergeret, P. Gallezot and F. Lefebvre, in: *New Developments in Zeolite Science and Technology*, eds. Y. Murakami, A. Iijima and J.W. Ward, (Elsevier, Amsterdam, 1986) pp. 401–408.
[14] P. Gelin, C. Naccache, Y. Ben Taârit and Y. Diab, Nouv. J. Chim. 8 (1983) 675.
[15] P. Gelin, F. Lefebvre, B. Elleuch, C. Naccache and Y. Ben Taârit, in: *Intrazeolite Chemistry*, eds. G.D. Stucky and F.G. Dwyer (ACS, Washington, 1983) p. 455.
[16] M. Dufaux, P. Gelin and C. Naccache, in: *Catalysis by Zeolites*, ed. B. Imelik (Elsevier, Amsterdam, 1980) pp. 261–271.
[17] S. Kawi, J.-R. Chang and B.C. Gates, J. Am. Chem. Soc. 115 (1993) 4830.
[18] D. Roberto, E. Cariati, R. Psaro and R. Ugo, Organometallics 13 (1994) 4227.
[19] P.D. Lane, PhD Thesis, University of Illinois at Urbana-Champaign, USA (1995).
[20] M.A. Urbancic, PhD Thesis, University of Illinois at Urbana-Champaign, USA (1984).
[21] P.A. Lee, P.H. Citrin, P. Eisenberger and B.M. Kincaid, Rev. Mod. Phys. 53 (1981) 769.
[22] B.K. Teo, *EXAFS: Basic Principles and Data Analysis* (Springer, New York, 1986).
[23] M.S. Nashner, D.S. Somerville, P.D. Lane, D.L. Adler, J.R. Shapley and R.G. Nuzzo, J. Am. Chem. Soc. 118 (1996) 12964.
[24] R.B. Greegor and F.W. Lytle, J. Catal. 63 (1980) 476.
[25] B.J. Kip, F.B.M. Duivenvoorden, D.C. Koningsberger and R. Prins, J. Catal. 105 (1987) 26.
[26] R.E. Benfield, J. Chem. Soc. Faraday Trans. 88 (1992) 1107.
[27] J.B.A.D. van Zon, D.C. Koningsberger, H.F.J. van't Blik and D.E. Sayers, J. Chem. Phys. 82 (1985) 5742.
[28] B.S. Clausen, L. Grabek, H. Topsøe, L.B. Hansen, P. Stoltze, J.K. Norskøv and O.H. Nielsen, J. Catal. 141 (1993) 368.
[29] J.H. Sinfelt, G.H. Via and F.W. Lytle, Catal. Rev. Sci. Eng. 26 (1984) 81.
[30] (a) F.B.M. van Zon, PhD Thesis, Eindhoven University, The Netherlands (1988);
(b) N.D. Triantafillou, J.T. Miller and B.C. Gates, J. Catal. 155 (1995) 131.
[31] N.D. Triantafillou, S.E. Deutsch, O. Alexeev, J.T. Miller and B.C. Gates, J. Catal. 159 (1996) 14.
[32] S. Kawi and B.C. Gates, J. Phys. Chem. 99 (1995) 8824.
[33] G.B. McVicker, R.T.K. Baker, R.L. Garten and E.L. Kugler, J. Catal. 65 (1980) 207.
[34] M.J. Kappers, J.T. Miller and D.C. Koningsberger, J. Phys. Chem. 100 (1996) 227.
[35] L.-L. Sheu, H. Knözinger and W.M.H. Sachtler, J. Am. Chem. Soc. 111 (1989) 8125.
[36] G.H. Via, J.H. Sinfelt and F.W. Lytle, J. Chem. Phys. 71 (1979) 690.
[37] J.H. Sinfelt, G.H. Via and F.W. Lytle, Catal. Rev. Sci. Eng. 26 (1984) 81.
[38] (a) G. Meitzner, G.H. Via, F.W. Lytle and J.H. Sinfelt, J. Phys. Chem. 96 (1992) 4960;
(b) J.H. Sinfelt and G.D. Meitzner, Acc. Chem. Res. (1993) 1.
[39] F.B.M. van Zon, S.D. Maloney, B.C. Gates and D.C. Koningsberger, J. Am. Chem. Soc. 115 (1993) 10317.
[40] K. Foger and J.R. Anderson, J. Catal. 59 (1979) 325.
[41] D.E. Resasco and G.L. Haller, J. Phys. Chem. 88 (1984) 4552.
[42] K. Foger and H. Jaeger, J. Catal. 120 (1989) 465.
[43] J.R. Engstrom, D.W. Goodman and W.H. Weinberg, J. Am. Chem. Soc. 110 (1988) 8305.
[44] K. Foger, J. Catal. 78 (1982) 406.
[45] T.C. Wong, L.F. Brown and G.L. Haller, J. Chem. Soc. Faraday Trans. I 71 (1981) 519.
[46] (a) M. Ichikawa, L.-F. Rao, T. Kimura and A. Fukuoka, J. Mol. Catal. 62 (1990) 15;
(b) M. Ichikawa, L. Rao, T. Ito and A. Fukuoka, Faraday Discuss. Chem. Soc. 87 (1989) 321.
[47] (a) J.R. Shapley, S.J. Hardwick, D.S. Foose, G.D. Stucky, M.R. Churchill, C. Bueno and J.P. Hutchinson, J. Am. Chem. Soc. 103 (1981) 7383;
(b) J.R. Shapley, W.S. Uchiyama and R.A. Scott, J. Phys. Chem. 94 (1990) 1190.
[48] D.F. Johnson and W.H. Weinberg, J. Chem. Soc. Faraday Trans. 91 (1995) 3695.
[49] K. Foger and J.R. Anderson, J. Catal. 64 (1980) 448.
[50] J.H. Sinfelt, *Bimetallic Catalysts – Discoveries, Concepts, and Applications* (Wiley, New York, 1983).
[51] G.A. Martin, Catal. Rev. Sci. Eng. 30 (1988) 519.
[52] B. Chen and J.G. Goodwin, J. Catal. 158 (1996) 228.
[53] Y.H. Romdhane, B. Bellamy, A. de Gouveia and M. Che, Appl. Surf. Sci. 31 (1988) 55.
[54] J.A. Dalmon and G.A. Martin, J. Catal. 66 (1980) 214.
[55] S.T. Homeyer, Z. Karpinski and W.M.H. Sachtler, J. Catal. 123 (1990) 60.
[56] S. Kawi, J.-R. Chang and B.C. Gates, J. Phys. Chem. 98 (1994) 12978.
[57] Z. Xu, F.-S. Xiao, S.K. Purnell, O. Alexeev, S. Kawi, S.E. Deutsch and B.C. Gates, Nature 372 (1994) 346.